International Immunology, Vol. 34, No. 4, pp. 207–223
https://doi.org/10.1093/intimm/dxab111
Advance Access publication 1 December 2021

Multiple tolerance checkpoints restrain affinity maturation of B cells expressing the germline precursor of a lupus patient-derived anti-dsDNA antibody in knock-in mice

Marwa Ali El Hussien[1], Chao-Yuan Tsai[1], Yuhkoh Satouh[2,6], Daisuke Motooka[3,4], Daisuke Okuzaki[3,4], Masahito Ikawa[5], Hitoshi Kikutani[1] and **Shuhei Sakakibara[1]**

[1]Laboratory of Immune Regulation, Immunology Frontier Research Center, Osaka University, Osaka 565-0871, Japan
[2]Animal Resource Center for Infectious Diseases, Research Institute for Microbial Diseases, Osaka University, Osaka 565-0871, Japan
[3]Laboratory of Human Immunology, Immunology Frontier Research Center, Osaka University, Osaka 565-0871, Japan
[4]Genome Information Research Center, Research Institute for Microbial Diseases, Osaka University, Suita, Osaka 565-0871, Japan
[5]Department of Experimental Genome Research, Research Institute for Microbial Diseases, Osaka University, Osaka 565-0871, Japan
[6]Present address: Laboratory of Molecular Traffic, Department of Molecular and Cellular Biology, Institute for Molecular and Cellular Regulation, Gunma University, Gunma 371-8512, Japan

Correspondence to: H. Kikutani; E-mail: kikutani@biken.osaka-u.ac.jp or S. Sakakibara; E-mail: sakakibara@ifrec.osaka-u.ac.jp

Received 14 September 2021, *editorial decision* 26 November 2021; *accepted* 27 November 2021

Abstract

Anti-dsDNA antibodies are a hallmark of systemic lupus erythematosus and are highly associated with its exacerbation. Cumulative evidence has suggested that somatic hypermutation contributes to the high-affinity reactivity of anti-dsDNA antibodies. Our previous study demonstrated that these antibodies are generated from germline precursors with low-affinity ssDNA reactivity through affinity maturation and clonal expansion in patients with acute lupus. This raised the question of whether such precursors could be subjected to immune tolerance. To address this, we generated a site-directed knock-in (KI) mouse line, G9gl, which carries germline-reverted sequences of the V_H–D_H–J_H and Vκ–Jκ regions of patient-derived, high-affinity anti-dsDNA antibodies. G9gl heterozygous mice had a reduced number of peripheral B cells, only 27% of which expressed G9gl B-cell receptor (BCR). The remaining B cells harbored non-KI allele-derived immunoglobulin heavy (IgH) chains or fusion products of upstream mouse V_H and the KI gene, suggesting that receptor editing through V_H replacement occurred in a large proportion of B cells in the KI mice. G9gl BCR-expressing B cells responded to ssDNA but not dsDNA, and exhibited several anergic phenotypes, including reduced surface BCR and shortened life span. Furthermore, G9gl B cells were excluded from germinal centers (GCs) induced by several conditions. In particular, following immunization with methylated bovine serum albumin-conjugated bacterial DNA, G9gl B cells occurred at a high frequency in memory B cells but not GC B cells or plasmablasts. Collectively, multiple tolerance checkpoints prevented low-affinity precursors of pathogenic anti-dsDNA B cells from undergoing clonal expansion and affinity maturation in GCs.

Keywords: anti-dsDNA antibodies, B-cell tolerance, systemic lupus erythematosus

Introduction

Systemic lupus erythematosus (SLE) is a life-threatening autoimmune disease that affects various organs and tissues. Sera of SLE patients contain high titers of autoantibodies, including anti-nuclear antibodies (ANAs), that form a pathogenic immune complex to induce complement-dependent inflammation. Among these autoantibodies, anti-dsDNA antibodies are highly specific for SLE and serum titers of anti-dsDNA IgG are correlated with SLE exacerbation (1, 2). In contrast, anti-ssDNA antibodies are less specific for the disease (3, 4).

We previously generated several anti-DNA recombinant monoclonal antibodies from peripheral plasmablasts of acute SLE patients. These antibodies could not only bind to both ssDNA and dsDNA at high affinity, but also show typical anti-nuclear staining (5). The crystallographic analysis also revealed that these anti-dsDNA antibodies target nucleobases through stacking interaction with aromatic residues in complementarity-determining regions (CDRs) (5), a process that is structurally homologous to antigen recognition by anti-ssDNA monoclonal antibodies derived from autoimmune disease-prone mice (6, 7). Moreover, we have demonstrated that high-affinity binding of anti-DNA clones to dsDNA was facilitated by their robust ability to dissociate DNA strands from the double helix and to expose nucleobases (5). These observations strongly suggested that some anti-dsDNA antibodies of SLE patients are high-affinity anti-ssDNA antibodies.

Consistent with other studies (8–10), our high-throughput immunoglobulin (Ig) sequencing indicated that clonal diversification and selection of anti-dsDNA antibodies occurred in acute SLE (5). In both mice and humans, somatic mutations that confer the ability to bind to dsDNA often increased anti-ssDNA reactivity simultaneously (8–10). We have shown that the germline antibody encoded by reversely mutated Igs of the SLE-derived human anti-dsDNA clone 71F12 exhibited weak but detectable binding to ssDNA (5). Thus, pathogenic anti-dsDNA antibodies in SLE patients could originate from precursors with low-affinity ssDNA reactivity through affinity maturation.

It has been shown that anti-dsDNA B cells were suppressed by multiple tolerance mechanisms in mouse models (11–14). Although some dsDNA-reactive B cells were deleted in bone marrow, many emigrated to the periphery and exhibited an altered surface phenotype and reduced lifespan (13, 15, 16). Most of these studies used pre-rearranged Ig transgenic (Tg) and site-directed knock-in (KI) mice carrying high-affinity anti-dsDNA Igs from autoimmune mice. Thus, it still remains unclear whether the unmutated low-affinity precursor B cells of SLE-related pathogenic anti-dsDNA B cells and plasma cells can be suppressed by similar mechanisms in healthy conditions and how the precursor B cells differentiate into high-affinity anti-dsDNA B cells and PBs in SLE patients.

In this study, we sought to characterize the fate of precursors of pathogenic anti-dsDNA B cells and plasma cells that are generated in acute SLE patients. To this end, we developed a B-cell receptor (BCR) KI mouse line that carries the germline-reverted rearranged V_H–D_H–J_H and Vκ–Jκ sequences of 121G9, one of the lupus patient-derived high-affinity anti-DNA antibodies that are reactive to both dsDNA and ssDNA (5). We used the 121G9 germline sequence for BCR KI mice because the germline-reverted antibody completely lost anti-dsDNA reactivity but retained anti-ssDNA reactivity, albeit with 300-fold lower activity than that of the original 121G9 antibody. We found that expansion and antigen-driven affinity maturation of G9gl KI BCR-expressing B cells were hindered by the mechanisms that maintain immune tolerance. This work defines tolerance checkpoints for precursor B cells that express germline Igs of disease-associated anti-dsDNA antibodies.

Methods

Animals

All animal care was performed in accordance with the institutional guidelines of the RIMD/IFReC Animal Care and Use committees at Osaka University. G9gl site-directed KI mice were obtained as described in the below section. *Tlr9* knockout mice (17) were provided by Dr S. Akira (Osaka University). *Foxp3*-DTR-GFP mice (18) were originally established by Dr A. Rudensky (Memorial Sloan Kettering Cancer Center). B6.*Igh*^{a} congenic mice (No. 001317) were originally established by Jackson Laboratory, Bar Harbor, ME, and the frozen embryos (RBRC01201) were obtained from Riken Bioresource Center, Ibaraki, Japan. *Rag2*$^{-/-}$ mice were purchased from Jackson Laboratory. B1-8^{hi} KI mice (19) were provided by Dr M. Nussenzweig (Rockefeller University). B6 *Fas*$^{lpr/lpr}$ mice were purchased from SLC, Shizuoka, Japan.

Generation of G9gl BCR KI mice

The CRISPR/Cas9 plasmid px459 (Addgene) was digested with *Bbs* I (NEB) for insertion with the gRNA cassette as described elsewhere (20, 21). For gene editing of the Ig heavy (IgH) chain locus, px459-ch12-2-2 [CAAGAGATGACTGGCAGATT*GGG* (the PAM sequence is shown in italics)] and px459-ch12-2b-3 (TACTATGCTAT GGACTACTG*GGG*) were co-transfected with the targeting vector pCR2.1-Ch12-121G9, which contained ~2-kb homologous arms at the 5′ and 3′ ends of the 121G9GL IgH VDJ transgene, into C57BL/6 (B6) ES cells with EGFP as a reporter (22). For the light (L) chain (Igκ) locus, px459-ch6-4-2 (CCACTGTGGTGGACGTTCGG*TGG*) and px459-ch6-4b-1 (TGTGGCTCACGTTCGGTGCT*GGG*) were co-transfected with the targeting vector pCR2.1-Ch6-121G9, which contained homologous arms at both sides of the transgene. ES clones with successful recombination were first screened by PCR and confirmed by direct DNA sequencing. Selected ES clones were injected into eight-cell embryos of pseudopregnant ICR female mice (Clea Japan, Inc.) to obtain chimeric mice, which were crossed with B6 (Clea Japan, Inc.). Mice carrying the G9gl H and L chains were intercrossed. G9gl HL homozygous mice were bred with these mice to obtain G9gl HL *Tlr9*$^{-/-}$, G9gl HL *Foxp3*^{DTR}, G9gl HL × *Igh*^{a}, and G9gl HL *Rag2*$^{-/-}$ mice.

Calcium influx assay

The calcium influx assay was performed as described elsewhere (23) with slight modifications. Single suspensions of splenocytes were prepared from 7 -to 8-week-old G9gl HL homozygous mice or control mice and were stained with APCCy7-conjugated anti-B220 antibody (Biolegend). The stained cells were further incubated with complete RPMI 1640 (Fujifilm) containing 1× loading dye from a BD Calcium Assay Kit according to the manufacturer's instructions. The dye-loaded cells were equilibrated at room temperature and a FACS Canto II (BD) was used to record background signals for 1 min. After recording of the basal signal, cells were stimulated with 10 μg/ml of anti-IgM F(ab')$_2$ (Southern Biotech), 1 or 0.5 μg/ml of ssDNA, or dsDNA and then immediately placed on the FACS machine. Signals were collected for 20 min. The

obtained data were analyzed using FlowJo software (Tree Star).

Flow cytometry

Single-cell suspensions of splenocytes were prepared and stained as described elsewhere (24). Bone marrow cells were obtained from hind leg femurs. The following antibodies and reagents were used: APCCy7-conjugated anti-IgD, violetFluor450-conjugated anti-B220, AlexaFluor647- or FITC-conjugated GL7, APC-conjugated anti-CD43 (from BioLegend); APC-conjugated anti-IgM, PE-conjugated anti-IgM^a, biotin-conjugated anti-IgM^b, biotin-conjugated anti-Igκ, APC-conjugated anti-$Igλ_{1/2/3}$, PECy7-conjugated anti-CD21, PECy7-conjugated anti-CD38, APC-conjugated anti-CD45.1, PE-conjugated anti-CD45.2, PE-conjugated anti-IgG_1, biotin-conjugated anti-$IgG_{2a/2b}$, biotin-conjugated anti-IgG_3, FITC-conjugated anti-CD93, PE-conjugated CD268 (BAFFR), PE-conjugated CD267 (TACI) (from BD); PE-conjugated anti-CD23, FITC-conjugated Y-Ae (from Thermo Fisher). Cells were incubation with antibodies on ice after the Fc blocking procedure with the 2.4G2 antibody (Tonbo). 7AAD (BioLegend) was used to stain dead cells in the analysis. For intracellular staining of AKT, phosphorylated CD79a, and SHIP1, cells were stained by antibody against surface markers and then fixed and permeabilized with Cytofix/Cytoperm (BD) to be reacted with and rabbit anti-AKT (Cell Signaling Technology), anti-phosphorylated CD79a (Tyr 182) (Cell Signaling Technology), or anti-SHIP1 (Abcam) followed by Alexa647-conjugated anti-rabbit IgG (Thermo Fisher). Flow cytometric analysis was performed on a FACS CantoII, and obtained data were analyzed using FlowJo software (Tree Star).

Bulk IgH sequencing for the detection of VH rearrangement

Non-G9gl KI IgH allele-expressing B cells (IgM^{a+} IgM^{b-} $B220^+$) in G9gl HL heterozygous mice were sorted using a FACS Aria (BD). The sorted cells (~1 million cells) were lysed in Tris–EDTA buffer with 1% SDS and proteinase K (Nacalai) and then incubated at 65°C for 4 h. Genomic DNA was isolated by phenol/chloroform extraction followed by isopropanol precipitation. We designed forward and reverse primers that targeted the 5′ ends of the mouse V_H and J_H regions of the G9gl H chain, respectively: 5′ mIgG-Fw-Not (5′-AAAGCGG CCGCCTCTGAGGTGCAGCTGCAGGAGTCTGG-3′) and 3′ huJ_H4-Sal (5′-TGCGAAGTCGACGCTGAGGAGACGGTGAC CAG). The amplicons (~500 bp) were digested with *Not* I and *Sal* I (Toyobo), and then agarose gel-purified for subcloning into the pFLAGCMV14 plasmid (Sigma). After transduction into *E. coli* DH5α (Nippon Gene), ampicillin-resistant colonies were obtained on LB agar plates. The sequences of individual colonies were determined by Sanger DNA sequencing.

Antigen uptake assay

Isolated splenocytes (1×10^6) from control and G9gl HL homozygous mice were incubated with 2 μg/ml of biotin-conjugated goat anti-mouse IgM $F(ab')_2$ (Southern Biotech) for 10 min on ice. After incubation, these cells were washed thrice with ice-cold PBS; some were then kept on ice and the remainder were cultured in RPMI 1640 supplemented with 10% heat-inactivated FBS (Thermo Fisher), 2 mM of L-glutamine (Nacalai), non-essential amino acids (Thermo Fisher), sodium pyruvate (Thermo Fisher), 50 μM of 2-mercaptoethanol (Thermo Fisher) for 1 h. All cells were stained with 7AAD, violetFluor450-conjugated anti-B220 antibody, and PE-conjugated streptavidin, and analyzed by flow cytometry. The percent remaining anti-IgM signal intensity among $7AAD^-$ $B220^+$ cells was calculated.

Antigen presentation assay

$Eα^{52–68}$ peptide (Anaspec) was conjugated with goat anti-mouse IgM $F(ab')_2$ by 1-ethyl-3-(3-dimethylaminopropyl) carbodiimide hydrochloride (Thermo Fisher) according to the manufacturer's protocol. Isolated splenocytes (1×10^6) from control and G9gl KI mice were cultured in complete RPMI containing 7.5 μg/ml of the anti-IgM $F(ab')_2$-$Eα^{52–68}$ conjugates for 16 h. After washing, these cells were stained with 7AAD, anti-B220 antibody and Y-Ae, the last of which specifically recognizes the $I\text{-}A^b$ and $Eα^{52–68}$ peptide complex. The median fluorescent intensity of the stained cells was measured by flow cytometry.

In vitro stimulation assay

To prepare unmethylated CpG motif-containing ssDNA, plasmid DNA [pcDNA3 (Invitrogen)] was prepared using a PureLink Maxiprep Kit (Thermo Fisher) and linearized by EcoRI (Takara). The linearized plasmid DNA was phenol/chloroform-extracted and treated with Endotoxin Removal Solution (Sigma) according to the manufacturer's protocol. After endotoxin removal, plasmids were heat denatured. Fo B cells ($B220^+$ $CD93^-$ $CD21^{lo}$ $CD23^{hi}$) were sorted from splenocytes of 7-week-old WT and G9gl HL homozygous mice. NP-specific Fo B cells ($B220^+$ $CD93^-$ $CD21^{lo}$ $CD23^{hi}$ Igκ–) were sorted from splenocytes of 7-week-old $B1\text{-}8^{hi}$ KI mice. For evaluation of cell proliferation, sorted B cells were stained with CellTracker Violet (Thermo Fisher) according to the manufacturer's instructions. CTV-stained splenic Fo B cells were incubated in 24- or 48-well plates at 0.5–1 million cells/well. For stimulation of B cells, 5 μg/ml of anti-CD40 antibody (BioLegend), 50 ng/ml of IL-4 (R&D) and 10 ng/ml of IL-5 (R&D) were added to complete RPMI1640 medium supplemented with heat-inactivated 10% FBS. For ssDNA stimulation, 1 μg/ml of linearized and denatured, endotoxin-free plasmid DNA was added into the culture condition. To antagonize TLR9, 1 μM of ODN2088 (Invivogen) was added to the culture 1 h before ssDNA stimulation. The cells were cultured at 37°C in a humidified incubator in an atmosphere of 10% CO_2 for 4 days before FACS analysis.

Measurement of early and late apoptosis in B cells

Mature Fo B cells ($B220^+$ $CD93^-$ $CD21^{lo}$ $CD23^{hi}$) were sorted from splenocytes of 7- to 9-week-old B6 or G9gl HL *Rag2*$^{-/-}$ mice. The sorted B cells were washed twice in complete RPMI and cultured in the presence or absence of 10 ng/ml of mouse recombinant BAFF (R&D). After 24-h culture, B cells were harvested, washed in PBS and then incubated in binding buffer [10 mM HEPES (pH 7.4), 140 mM NaCl, 0.25 mM $CaCl_2$] with FITC-conjugated annexin V (BD) and 7AAD (BD) at room

temperature for 15 min. Stained cells were diluted in binding buffer immediately before flow cytometric analysis.

Single-cell Ig sequencing and recombinant antibody expression

Single-cell Ig cloning was performed as described previously (25, 26). Briefly, IgG$^+$ GC B (B220$^+$ CD38^{lo} GL7^{hi} IgG$_{1,2b/c,or\ 3}^+$), IgG$^+$ memory B cells (B220$^+$ CD38^{hi} GL7$^-$ IgG$_{1,2b/c,or\ 3}^+$) or IgG$^+$ plasmablasts (B220$^{lo/+}$ CD138$^+$ IgG$_{1,2b/c,or\ 3}^+$) were sorted by FACS Aria III (BD). cDNA was synthesized by SuperScript™ II reverse transcriptase (Thermo Fisher) with random primers (Thermo Fisher). Primers for the first PCR were designed for amplification of mouse IgG transcripts composed of different V_H–D_H–J_H combinations (25, 26). After nested RT-PCR, amplified fragments were agarose gel-purified. Sanger sequencing was performed for each fragment and obtained sequences were analyzed using IMGT/V-QUEST (27). For expression of recombinant monoclonal antibodies, amplified V regions of H and L chains were sub-cloned into expression vectors for mouse IgG and Igκ, respectively. The H and L chain plasmids were co-transfected into HEK293T cells with polyethyleneimine (Polysciences).

Hep2 staining

Mouse sera were diluted in 0.1% BSA-containing PBS. For recombinant monoclonal antibodies, the antibody concentration of culture supernatant from each transfectant was adjusted to 2 μg/ml. Diluted sera (1:100) and culture supernatant were tested in an indirect immunofluorescent assay with glass slides of Hep2 cells (Bio-Rad). Bound antibodies were detected by anti-mouse IgG-Alexa Fluor 488 antibody (Thermo Fisher). After washing, sections were mounted with Fluoro-KEEPER Antifade mounting medium (Nacalai) and observed on FluoView FV1000 (Olympus). Pseudocolored images were converted into TIFF files by using Olympus FV software.

ELISA

Serum anti-dsDNA or anti-ssDNA IgG titers were determined by ELISA as described elsewhere (28). In brief, for dsDNA, DNA from calf thymus (Sigma) was sonicated to below 3 kbp in size and treated with 1 U/μg S1 nuclease (Takara) for 30 min at 37°C. DNA was purified with TE-saturated phenol and ethanol precipitated. For ssDNA, dsDNA was heat-denatured at 95°C for 5 min followed by immediate incubation on ice for 1 min. An ELISA plate (Nunc) was coated with dsDNA or ssDNA (10 μg/ml) in PBS overnight at 4°C. After brief washing with PBST, the plate was blocked with PBS containing 1% Ig-free BSA (Nacalai) for 1 h. After washing twice with PBST, the plates were filled with serial dilutions of sera in PBS with 0.1% BSA and incubated at RT for 2 h. HRP-conjugated secondary antibodies (Southern Biotech) were used for detection. For sera from mice immunized with mBSA-conjugated bacterial DNA, ELISA plates were blocked by 1% ovalbumin instead of BSA.121G9 antibody (5) with a mouse IgG$_{2a}$/Igκ Fc region was used as a standard for anti-dsDNA, and serum anti-dsDNA titers were expressed as arbitrary units. For detection of anti-dsDNA IgG$_{2a}$ and IgG$_{2c}$, HRP-conjugated goat anti-mouse IgG$_{2a}$ and anti-mouse IgG$_{2c}$ antibodies (Southern Biotech) were used in 1:4000 dilution. For serum IgG against nuclear antigens, an ANA Screen 8 ELISA Kit (Orientec) was used according to the manufacturer's instruction. Anti-Smith antigen monoclonal antibody 51F1 (5) with a mouse IgG$_{2a}$/Igλ constant region was used as a standard and serum ANA titer were expressed as arbitrary units.

Adoptive transfer

Pan B cells (CD43 negative) from splenocytes of WT or G9gl HL *Rag2*$^{-/-}$ mice (CD45.1) were sorted by an Aria III (BD). One million cells in 100 μl of PBS containing 0.063% of anti-coagulant citrate dextrose (Sigma) were transferred into recipient mice (CD45.2) by retro-orbital injections. At each time point, spleens were isolated and then donor-derived splenic cells (B220$^+$ CD45.1$^+$ CD45.2$^-$) were detected by flow cytometry. The absolute numbers of donor-derived cells were calculated. The half-life of wild-type (WT) or G9gl B cells was calculated by GraphPad (Prism).

RNAseq

Splenic Fo B cells were sorted by gating the B220$^+$ CD93$^-$ CD21^{lo} CD23^{hi} fraction from 8-week-old B6 control and G9gl homozygous mice. Total RNA was extracted using Trizol (Thermo Fisher) following the manufacturer's instructions. Full-length cDNA was generated using a SMART-Seq HT Kit (Takara Bio) according to the manufacturer's instructions. An Illumina library was prepared using a Nextera XT DNA Library Prep Kit (Illumina) according to SMARTer kit instructions. Sequencing was performed on an Illumina HiSeq 3000 sequencer (Illumina) in the 100-base paired-end mode. Expression analysis were performed as described previously (29). GSEA was performed using GSEA software (30, 31). The upstream regulator analysis was performed with IPA software (Qiagen) (32). The raw data are available at Gene Expression Omnibus (GEO) (accession number GSE183827).

Depletion of regulatory T cells in G9gl HL Foxp3^{DTR} *mice*

Seven- to 8-week-old G9gl HL *Foxp3*^{DTR} mice or control *Foxp3*^{DTR} mice were intraperitoneally (i.p.) injected with 1 μg of diphtheria toxin (DTx) (Fujifilm) in 100 μl of PBS at days 1, 4 and 7. Splenocytes were analyzed at days 10 and 24. Sera were collected at days 0, 10, 17 and 24 for ELISA and at day 24 for Hep2 staining. The BCR repertoire of IgG$^+$ GC B cells (7AAD$^-$ B220$^+$ CD38^{lo} GL7^{hi} IgG$_{1,2b/c\ or\ 3}^+$), IgG$^+$ memory B cells (7AAD$^-$ B220$^+$ CD38^{hi} GL7$^-$ IgG$_{1,2b/c\ or\ 3}^+$) and IgG$^+$ PBs (7AAD$^-$ B220$^{+/lo}$ CD138$^+$ IgG$_{1,2b/c\ or\ 3}^+$) from spleens of DTx-treated mice (day 24) were determined by single-cell Ig sequencing (scIg-seq) as described above.

Methylated BSA-conjugated bacterial DNA immunization

Bacterial DNA immunization was performed as described previously (33) with minor modifications. Endotoxin-free plasmid DNA (pcDNA3) was prepared as described above. Plasmid DNA was fragmented by Ultrasonic Disruptor UD-201 (Tomy) to be <3 kb and heat-denatured. Twenty-five micrograms of methylated BSA (mBSA) (Sigma) and 100 μg of shared bacterial ssDNA were incubated in 100 μl of PBS. The mBSA–DNA complex was emulsified 1:1 in complete

Freund's adjuvant (CFA) (Sigma). Seven- to 8-week-old G9gl HL heterozygous mice, which did not show high anti-dsDNA IgG titers in sera, or control mice were immunized with mBSA-conjugated DNA/CFA at day 1, and boosted with mBSA-conjugated DNA at days 14 and 28. Sera were collected at days 0, 21 and 35 for ELISA and Hep2 staining. The BCR repertoire of IgG$^+$ GC B cells (7AAD$^-$ B220$^+$ CD38^{lo} GL7^{hi} IgG$_{1,2b/c\ or\ 3}^+$), IgG$^+$ memory B cells (7AAD$^-$ B220$^+$ CD38^{hi} GL7$^-$ IgG$_{1,2b/c\ or\ 3}^+$) and IgG$^+$ PBs (7AAD$^-$ B220$^{+/lo}$ CD138$^+$ IgG$_{1,2b/c\ or\ 3}^+$) at days 7 and 35 after immunization was determined by scIg-seq as described above.

Statistical analyses

P values were calculated by the Mann–Whitney *U*-tests (two-tailed) using Prism 5 software (Graphpad). *P* values of <0.05 were considered statistically significant.

Results

121G9gl, the germline antibody of SLE-derived high-affinity anti-dsDNA clone 121G9, exhibits no binding affinity to dsDNA but is still able to bind to ssDNA

An SLE patient-derived human monoclonal antibody, 121G9, showed high-affinity binding to both dsDNA and ssDNA (5). Somatic hypermutation resulted in three- and four-amino acid substitutions on the H and L chains, respectively (Fig. 1A and B). The somatically mutated residues were critical for the self-reactivity of 121G9 because the germline antibody, 121G9gl, showed dramatically reduced binding affinity to both dsDNA and ssDNA (Fig. 1B); specifically, 121G9gl had no measurable binding affinity to dsDNA in the concentration range of 0.0137–30 μg/ml in ELISA, but was still able to bind to ssDNA, albeit with about 300-fold weaker activity than that of the original 121G9 antibody (EC_{50}: 121G9gl, 9.95 μg/ml; 121G9, 0.0314 μg/ml). A Hep2 nuclear staining assay further confirmed the critical role of somatically mutated residues for the anti-nuclear reactivity of 121G9 (Fig. 1C). On the basis of these results, we used 121G9gl as an anti-ssDNA germline Ig to generate a BCR KI mouse that produced low-affinity anti-ssDNA precursor B cells with the evolutionary potential to become pathogenic anti-dsDNA antibody-producing cells.

Receptor editing by V_H replacement eliminates G9gl BCR in a large proportion of B cells in G9gl HL heterozygous mice

We generated a site-directed KI mouse line, designated G9gl, carrying the rearranged V_H–D_H–J_H and Vκ–Jκ regions of 121G9gl in the respective genetic loci (Supplementary Fig. S1). The numbers of splenic B cells were significantly reduced in both the G9gl HL heterozygous (G9gl H/+ L/+) and homozygous (G9gl H/H L/L) mice (Fig. 2A and B). The numbers of mature Fo B cells (B220$^+$ CD93$^-$ CD23^{hi} CD21^{lo}) in G9gl HL heterozygotes and homozygotes were reduced by 41% and 35% relative to those in WT mice, respectively (Fig. 2A). The numbers of marginal zone (MZ) B cells (B220$^+$ CD93$^-$ CD21^{hi} CD23^{lo}) in G9gl HL heterozygotes were similar to those of WT mice, whereas they were barely detected in G9gl HL homozygous mice (Fig. 2A). The numbers of immature B cells were also reduced in both G9gl HL heterozygous and homozygous mice (Fig. 2B). Transitional T3 cells (B220$^+$ CD93$^+$ CD23$^+$ IgM^{lo}), in which anergic self-reactive B cells are reportedly overrepresented in mice and humans (34), exhibited lower absolute numbers but higher frequencies in G9gl HL homozygous mice compared with WT mice (Fig. 2B). B-cell numbers were also reduced in the lymph nodes of both G9gl HL heterozygous and homozygous mice relative to WT mice (data not shown).

Targeted KI of pre-rearranged Ig segments results in dominance of KI BCR-expressing cells in the B-cell population because KI BCR expression triggers feedback suppression of rearrangement of the non-KI allele. We examined surface expression of KI allele-derived IgH chain relative to WT allele-derived IgH in G9gl HL heterozygous mice (G9gl HL [*Igh*^{b}] × B6.*Igh*^{a}). Unexpectedly, only about half of all B cells in heterozygous mice expressed G9gl BCR (IgM^{a-} IgM^{b+}), and the rest expressed WT allele-derived IgH (IgM^{a+} IgM^{b-}) (Fig. 2C). This suggests that receptor editing by V_H replacement might occur in G9gl HL KI mice, as previously shown in VH3H9 anti-dsDNA V_H–D_H–J_H KI mice (35). To confirm the occurrence of V_H replacement, we performed cloning and sequencing of the KI H chain gene locus in bulk-sorted B cells expressing WT allele-derived IgH (IgM^{a+} IgM^{b-}) from G9gl HL heterozygous mice. All of the obtained sequences encoded an aberrant fusion gene product in which the G9gl KI V_H was replaced with an upstream mouse V_H region, resulting in a frame shift at the junction (Supplementary Fig. S2). These observations indicated that B cells expressing WT allele IgH lost their G9gl V_H sequence as a result of receptor editing, which in turn caused a frame shift in the KI allele, followed by another rearrangement and expression of WT allele-derived IgH.

V_H replacement not only disrupts unwanted KI IgH, but also generates functional Igs (36). To verify the KI BCR expression, we performed scIg-seq. While Igλ$^+$ Igκ$^-$ B cells made up about 3% of B220$^+$ splenic cells in WT and G9gl HL heterozygous mice, these cells were almost completely absent in G9gl HL homozygous mice (Fig. 2D). Next, we performed single-cell sorting of Igλ$^-$ Fo B cells from the spleens of G9gl HL heterozygous and homozygous mice. In G9gl HL heterozygous mice, only about 27% of these cells expressed G9gl KI H chain (Fig. 2E). The remainder expressed either non-KI allele-derived IgH (56%) or edited IgH from the KI allele (17%), the latter of which is characterized by mouse V_H or V_H–D_H fused with G9gl D_H–J_H (Fig. 2E and F). Altogether, G9gl IgH was edited through V_H replacement in a large proportion of B cells in the KI heterozygous mice. On the other hand, more than 90% of Igλ$^-$ B cells expressed G9gl L chains in G9gl HL heterozygous mice and no edited L chain was detected (Fig. 2E). Almost all Fo B cells expressed G9gl H and L chains in G9gl HL homozygous mice (Fig. 2E), suggesting that the two homologous alleles of the KI H chain locus may be hardly replaced by receptor editing.

G9gl B cells are partially anergic and prone to cell death

G9gl HL heterozygous mice demonstrated a subpopulation of splenic B cells that exhibited lower expression of both IgM and IgD (Fig. 3A). This population was more predominant in G9gl HL homozygous mice (Fig. 3A), where most B cells expressed both G9gl H and L chains (Fig. 2E). In addition to reduced surface BCR, B cells in G9gl HL homozygous mice

A

```
                                          HCDR1                                HCDR2
121G9 H      1   QLQLQESGPG LVKPSETLSL TCTVSGGSIS SRSYYWGWIR QSPGKGLEWI GSIYYSGRT   60
121G9gl H    1   .......... .......... .......... .S........ .P........ .......S.   60

                                                                HCDR3
121G9 H     61   YYNPSLKSRV TISVDTSKNQ FSLKLSSVTA ADTAVYYCAR GVWGNYRYFD YWGQGTLVTV  120
121G9gl H   61   .......... .......... .......... .......... .......... ..........  120

                                    LCDR1                          LCDR2
121G9 k      1   DIQMTQSPSS LSASVGDRVT ITCRASQSIS SYLNWYQQKP GKAPKLLIYA ASSKSGVPS    60
121G9gl k    1   .......... .......... .......... .......... .......... ....Q.....   60
                                          HCDR3
121G9 k     61   RFSGSGSGTD FTLTISSLQP DDFTTYYCQQ SYSPPLTFGQ   100
121G9gl k   61   .......... .......... E..A...... ...T......   100
```

B

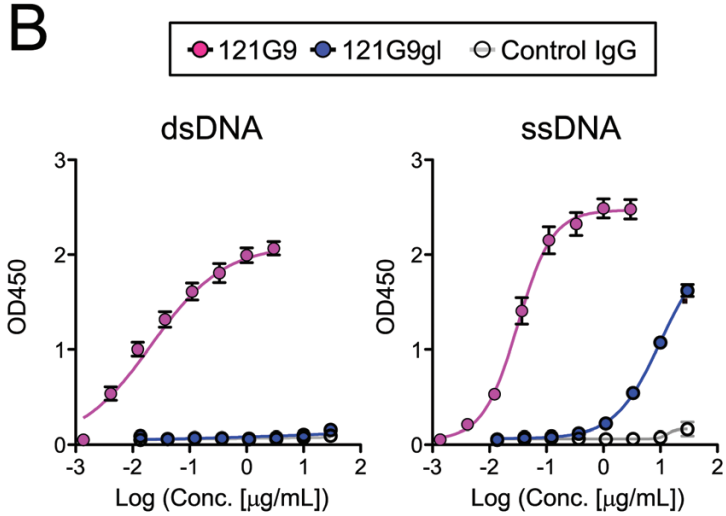

C

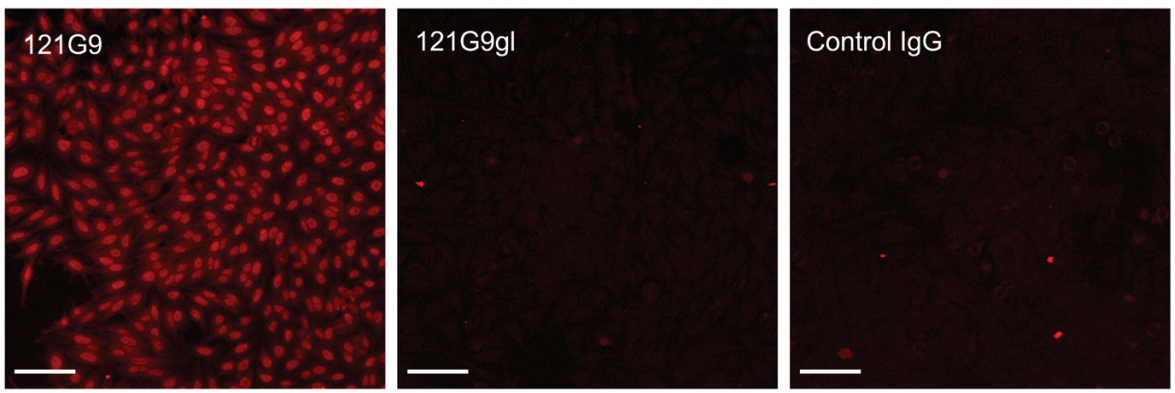

Fig. 1. 121G9gl, the germline antibody of high-affinity anti-dsDNA clone 121G9, exhibits no binding affinity to dsDNA but is still able to bind to ssDNA. (A) Amino acid sequence alignment of the variable regions from the H and L (κ) chains of anti-dsDNA clones 121G9 and 121G9gl. Identical amino acids are depicted by dots. (B) Binding of 121G9 (pink) and 121G9gl (blue) to dsDNA and ssDNA was assessed by ELISA. Each assay was carried out in duplicate. Representative results from three independent experiments are shown. (C) Hep2 staining assay. Anti-nuclear activity of 121G9 and 121G9gl was examined by Hep2 staining. The supernatants of transfectants with each IgG expression construct were adjusted to achieve an IgG concentration of 5 μg/ml and incubated on a Hep2 glass slide for 1 h at room temperature. Bound IgG was detected by anti-human IgG-Alexa Fluor 594-conjugated goat antibody. Bar indicates 100 μm. Representative results from two independent experiments are shown.

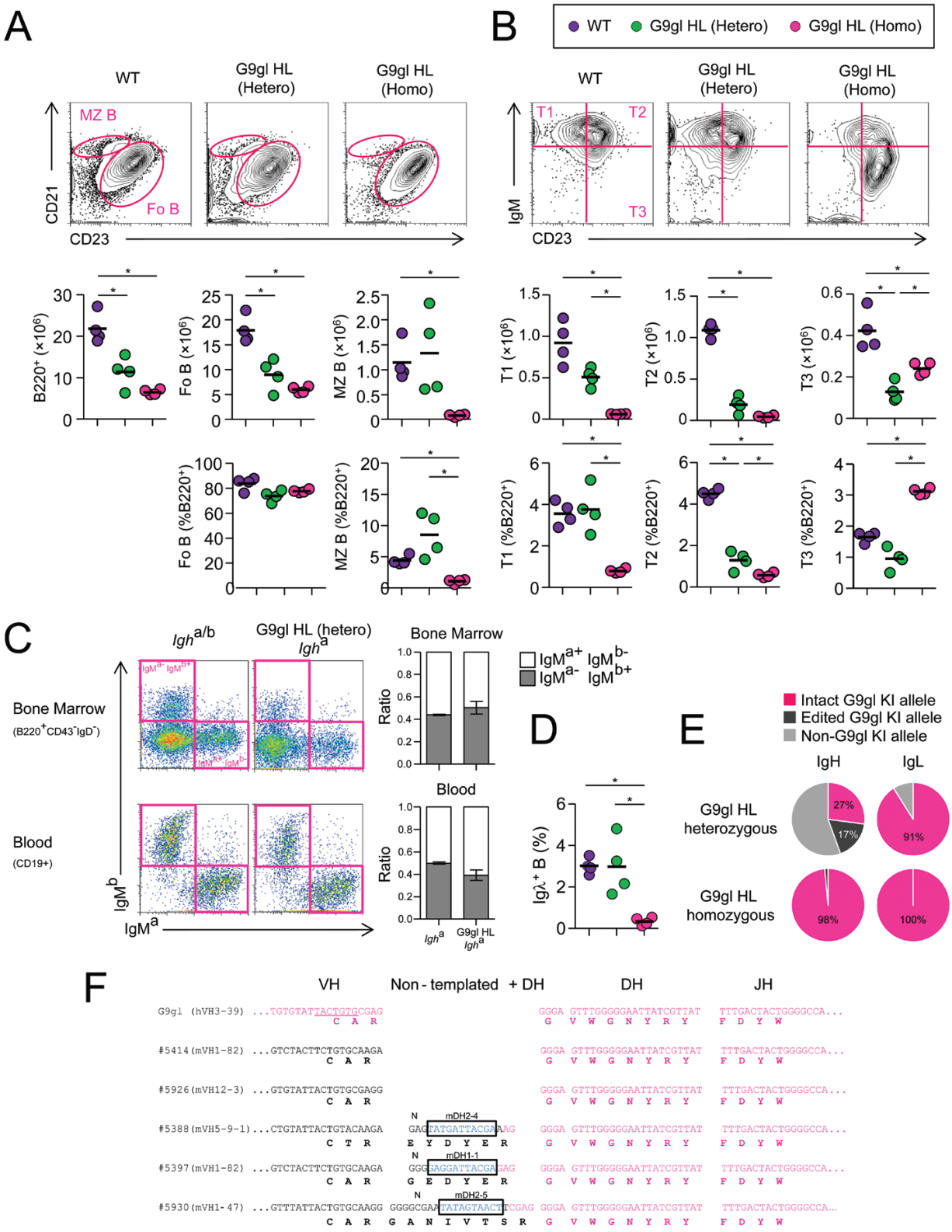

Fig. 2. B cells in spleens of G9gl HL KI mice are reduced in number. (A and B) Flow cytometric analysis of splenic B cells of 7-week-old WT, G9gl HL heterozygous, and homozygous mice. Representative FACS plots of 7AAD⁻ B220⁺ CD93⁻ mature (A) and 7AAD⁻ B220⁺ CD93⁺ transitional B cells (B) in the spleen are shown. The numbers and percentages of Fo, MZ and transitional B cells (T1, T2 and T3) in the spleens of 7-week-old WT (purple), G9gl HL heterozygous (green) and homozygous (pink) mice are shown the graphs. $n = 4$ each. Two-tailed Mann–Whitney test. $^*P < 0.05$. (C) Frequencies of IgH^{a+} and IgH^{b+} (B220⁺ CD43⁻ IgD⁻ IgM⁺) immature B cells among BM and blood CD19⁺ B cells

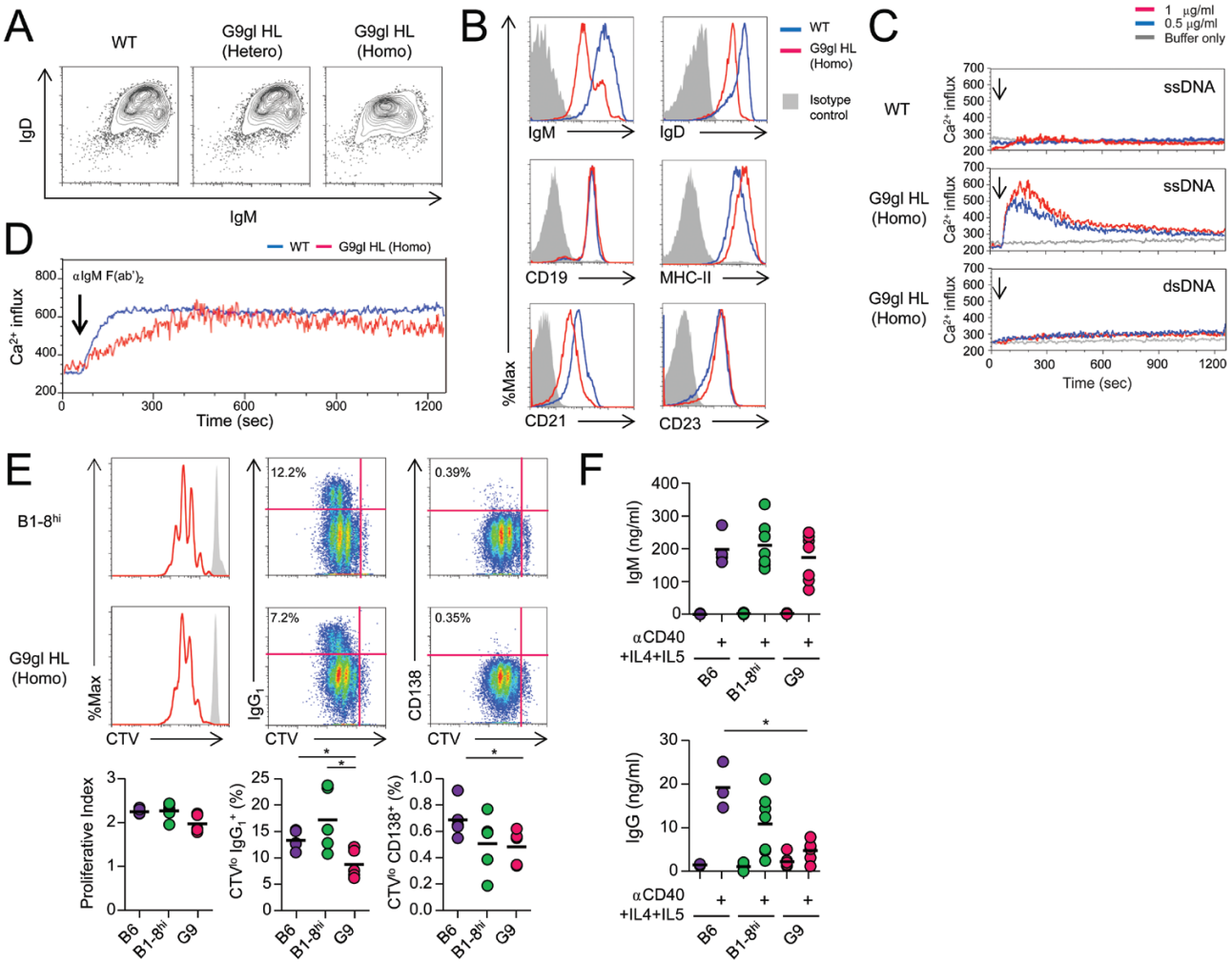

Fig. 3. G9gl B cells are partially anergic. (A) Surface expression of BCR on Fo B cells from WT and G9gl HL heterozygous and homozygous mice. Cells were stained with PE-conjugated anti-IgM and APCCy7-conjugated anti-IgD antibodies. Gating for 7AAD$^-$ B220$^+$ CD93$^-$. (B) Surface expression of IgM, IgD, CD19, MHC-II (I-A), CD21, and CD23. Gating for B220$^+$ CD93$^-$. Cells stained with isotype control antibody are shown in gray. (C and D) Calcium influx assay. Splenocytes were stained with APCCy7-conjugated anti-B220 and labeled with a calcium indicator. Then, cells were stimulated with ssDNA or dsDNA (C) or 10 μg/ml of anti-mouse IgM F(ab')$_2$ (D) at room temperature. Intracellular Ca^{2+} influx was monitored for 20 min by flow cytometry. The arrows indicate the time point of DNA or anti-mouse IgM F(ab')$_2$ addition. (E) *In vitro* stimulation of B cells from B6, B1-8^{hi}, or G9gl homozygous mice with anti-CD40 antibody, IL-4, and IL-5 for 4 days. Sorted Fo B cells were stained with CTV before stimulation. Harvested cells were stained with PE-conjugated anti-IgG$_1$ and APC-conjugated anti-CD138 antibodies. Proliferation indices were calculated by FlowJo software. n = 4-5. (F) Concentrations of IgM and IgG$_1$ in the culture supernatants of B6, B1-8^{hi} and G9gl homozygous mice were determined by ELISA. n = 3–7. (A–E) Data shown are representative of three to five independent experiments. (E and F) Two-tailed Mann–Whitney test. *P < 0.05.

had lower expression of CD21 and slightly higher expression of MHC-II (Fig. 3B). The expression levels of CD19 and CD23 were comparable in WT and G9gl B cells (Fig. 3B). Some of these surface phenotypes resembled those of anergic B cells in previously reported self-reactive BCR Tg mice (37).

We next stimulated B cells from homozygous G9gl HL mice with ssDNA or dsDNA *in vitro* to test whether G9gl BCR was functional. In a calcium influx assay, G9gl B cells could respond to ssDNA but not dsDNA (Fig. 3C), recapitulating the anti-DNA reactivity of 121G9gl in ELISA (Fig. 1B). Both control and G9gl B cells responded to BCR cross-linking by anti-IgM F(ab')$_2$, although the increase in signal intensity was slightly slower in G9gl B cells than WT B cells (Fig. 3D). This might be due to the reduced surface IgM expression on G9gl B cells. G9gl B cells were also able to incorporate a surrogate antigen, anti-IgM F(ab')$_2$, as efficiently as WT B

in WT *Igh*$^{a/b}$ and G9gl HL heterozygous mice (G9gl HL [*Igh*^{b}] x B6.*Igh*^{a}). The graphs show the IgM^{b+}/IgM^{a+} ratios. n = 3 each. (D) Frequencies of Igλ$^+$ cells in Fo B cells of WT (purple), G9gl HL heterozygous (green) and homozygous (pink) mice. n = 4. Two-tailed Mann–Whitney test. *P < 0.05. (E) Frequencies of Igλ$^-$ Fo B cells expressing IgH and IgL from intact G9gl KI allele, edited KI allele and non-KI allele in G9gl HL heterozygous and homozygous mice determined by scIg-seq. G9gl HL heterozygous (n = 2 mice, n = 59 H and L chains); homozygous mice (n = 2, n = 71). (F) Representative sequences of edited V_H–D_H–J_H regions encoding functional IgH from G9gl HL heterozygous mice.

cells (Supplementary Fig. S3A). They were also capable of antigen presentation through MHC-II (Supplementary Fig. S3B). These results indicated that G9gl B cells expressed functional BCR on the surface.

To further address whether G9gl B cells are able to respond to T-cell-derived stimuli, sorted Fo B cells were stimulated with anti-CD40 antibody, IL-4, and IL-5, then cultured for 4 d. As shown in Fig. 3E, G9gl B cells readily proliferated and underwent class switch recombination (CSR) and plasma cell differentiation, but CSR and subsequent differentiation were less efficient than control B cells from WT mice and hydroxy-3-nitrophenyl (NP) acetyl-hapten-reactive H-chain B1-8^{hi} KI mice. Although IgM secretion was comparable in G9gl and control B cells, G9gl B cells secreted significantly less IgG than control B cells (Fig. 3F), indicating that G9gl B cells are less effective at producing IgG antibodies in response to T-cell-derived stimuli. Thus, G9gl B cells are partially anergic, but still capable of performing most B-cell functions *in vitro*.

To gain insight into the unique anergic phenotype of G9gl B cells, we compared global gene expression in Fo B cells isolated from WT and G9gl HL homozygous mice. RNAseq analysis showed that 205 and 279 genes were downregulated and upregulated, respectively, in G9gl B cells relative to WT B cells (Fig. 4A). G9gl B cells demonstrated increased expression of *Jchain*, *Aicda* and *Mik67* (Fig. 4A), indicating that they were activated and proliferating. Upregulated genes in G9gl B cells also included *Apoe*, *Egr2*, *Lck*, *Marcksl1*, *Cd72* and *Cd83* (Supplementary Table S1), a finding that was consistent with a previous report on anergic self-reactive B cells from anti-HEL Ig and HEL double Tg mice (38). In gene set enrichment analysis (GSEA), the transcriptome of G9gl B cells was associated with an increase in gene sets related to cell cycle progression, such as E2F targets ($P < 0.001$, FDR $q = 0.150$), G2/M checkpoints ($P < 0.001$, FDR $q = 0.163$), and MYC targets ($P < 0.001$, FDR $q = 0.166$) (Fig. 4B and C). GSEA and Ingenuity upstream pathway analysis (IPA) (Supplementary Fig. S4A) indicated that G9gl B cells could be activated by the TLR-MYD88 pathway, IFNs, and IL-6. A central survival factor, *Akt1*, was downregulated 3.8-fold in G9gl B cells relative to control B cells (Supplementary Table S1). Intracellular staining confirmed that AKT protein expression was reduced in G9gl B cells compared to controls (Fig. 4D). In addition, the transcriptome of G9gl B cells exhibited weak correlation with pro-apoptotic gene expression, including Hallmark apoptosis ($P < 0.001$, FDR $q = 0.230$) and the p53 pathway ($P < 0.001$, FDR $q = 0.245$) (Fig. 4C and D). Indeed, G9gl B cells from G9gl HL *Rag2*$^{-/-}$ mice induced apoptotic cell death more rapidly than WT B cells in culture medium with no stimulators or mitogens (Fig. 4E). Soluble BAFF, an important survival factor for B cells, could sustain 50% survival of WT B cells relative to baseline at 24–48 h, but barely rescued G9gl B cells in the first 24 h (Fig. 4E). This may be partially due to reduced expression of BAFF receptors on G9gl B cells. BAFFR expression was reduced by 50% in G9gl B cells compared with WT B cells, although the expression level of TACI was comparable between G9gl B and WT B cells (Supplementary Fig. S4B). In concordance with the rapid cell death of G9gl B cells *in vitro*, these cells disappeared more rapidly from the spleen after adoptive transfer to B6 mice compared with WT B cells (Fig. 4F). The half-life of G9gl B cells in the spleen was approximately 33.1 h, which was 60% shorter than that of control B cells (83.5 h). RNAseq analysis and these experiments suggest that G9gl B cells are prone to cell death.

CpG motif-containing ssDNA enhances proliferation and CSR but inhibits plasma cell differentiation of G9gl B cells in vitro

Because the results of the RNAseq analysis suggested that TLR signaling could be activated in G9gl B cells (Supplementary Fig. S4), we examined the role of TLR9 in G9gl B cells. To this end, we crossbred G9gl HL mice with *Tlr9* knockout mice. The reduced number of splenic B cells and the anergic phenotype of G9gl B cells were still observed in G9gl HL homozygote mice lacking *Tlr9* (Supplementary Fig. S5A–C), indicating that suppression of G9gl B cells and their anergic phenotype are independent of TLR9-mediated signaling in healthy conditions. To assess the effect of CpG motif-containing ssDNA as a ligand for both G9gl BCR and TLR9, G9gl B cells were cultured with or without bacteria-derived ssDNA in the presence of anti-CD40 antibody, IL-4, and IL-5. The ssDNA augmented proliferation and enhanced CSR in G9gl B cells but not in WT or B1-8^{hi}/Igλ^{+} B cells (Fig. 5A). On the other hand, plasma cell differentiation of G9gl B cells was markedly downregulated by CpG-containing ssDNA, although B1-8^{hi}/Igλ^{+} B cells were not affected by the addition of NP-BSA under the same culture conditions (Fig. 5A). The TLR9 antagonist ODN2088 counteracted the acceleration of proliferation and the enhancement of CSR, but not the suppression of plasma cell differentiation of G9gl B cells by ssDNA (Fig. 5A). The proliferation and CSR of *Tlr9*-deficient G9gl B cells were unaffected by ssDNA, but their differentiation into plasma cells was still severely suppressed by CpG-containing ssDNA (Fig. 5B). These results suggest that TLR9 is required for enhancement of proliferation and CSR in G9gl B cells, but not for suppression of plasma cell differentiation induced by CpG-containing ssDNA. The precise mechanism for the suppressed plasma cell differentiation of G9gl B cells by ssDNA was unclear. CD79a Tyr182 phosphorylation was not dramatically increased in G9gl B cells after anti-IgM F(ab')$_2$ stimulation, although the phosphorylation level was slightly higher in G9gl B cells than WT B cells before stimulation (Fig. 5C). This was consistent with the inefficient calcium mobilization after BCR ligation (Fig. 2C). Nonetheless, expression of SHIP1, an essential lipid phosphatase for induction of anergy in self-reactive B cells (39) was lower in G9gl B cells than control B cells (Supplementary Fig. S5D). From the above results, plasma cell differentiation of G9gl B cells in response to CD40 cross-linking with IL-4 and IL-5 may be inhibited by altered BCR signaling independently of the TLR9-mediated pathway.

G9gl HL heterozygous mice spontaneously form germinal centers and produce autoantibodies independently of G9gl B cells

G9gl HL heterozygous mice started to produce anti-dsDNA antibodies at 2 months of age (Fig. 6A). Although aged control mice also produced substantial amounts of anti-dsDNA antibodies, serum titers of anti-dsDNA IgG were much higher in G9gl mice. Furthermore, in addition to anti-dsDNA and

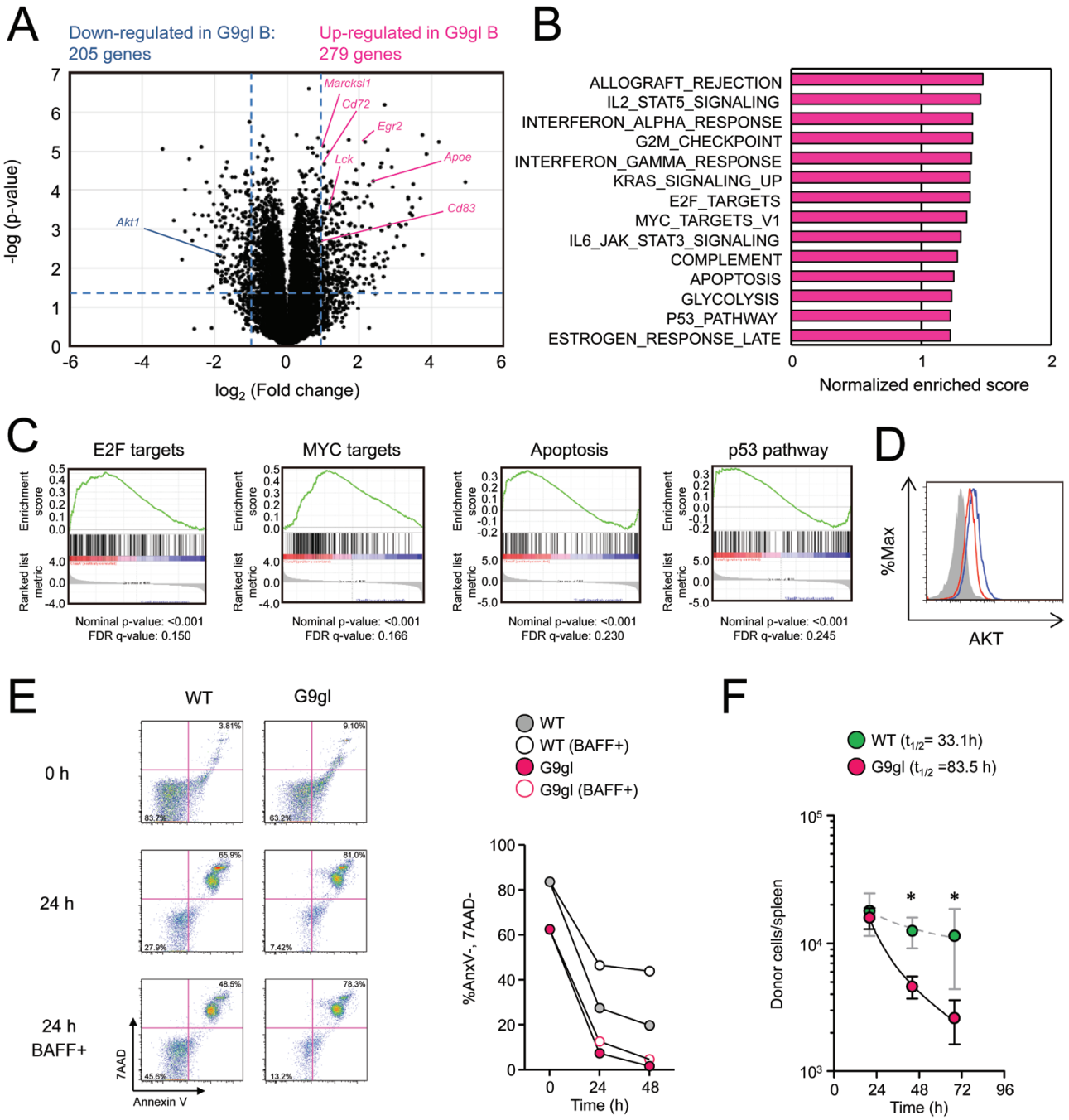

Fig. 4. G9gl B cells are prone to cell death. (A) Volcano plot of fold changes in gene expression levels in G9gl B cells relative to WT B cells. Fo B cells were sorted from 7-week-old WT or G9gl HL homozygous mice. (B) GSEA of upregulated genes in G9gl B cells (C) Representative GSEA results. Hallmark 'E2F targets', 'MYC targets', 'Apoptosis', and 'p53 pathway' are shown. (D) Intracellular staining of AKT expression on WT and G9gl B cells. Gating for Fo B (7AAD$^-$ B220$^+$ CD93$^-$ CD23^{hi} CD21^{lo}). Fluorescence minus one (FMO). Representative result from two independent experiments is shown. (E) Survival of WT and G9gl B cells *in vitro*. Sorted Fo B cells from WT and G9gl HL *Rag2*$^{-/-}$ mice were cultured in complete RPMI 1640 medium with 10% bovine fetal serum with or without BAFF (10 ng/ml). Representative FACS plots of live, early and late apoptotic cells detected by staining with annexin V and 7AAD. Gating for B220$^+$. The proportions of live cells (annexin V$^-$ 7AAD$^-$) are shown in the graph. Representative result from three independent experiments with three technical replicates is shown. (F) Numbers of transferred WT or G9gl B cells present in the spleen of recipient mice. Sorted splenic B cells (0.5 million cells) from WT CD45.1 or G9gl HL *Rag2*$^{-/-}$ CD45.1 mice were adoptively transferred into CD45.2 mice. Donor-derived B cells in the spleen were detected by CD45.1 and B220 and enumerated by flow cytometry. $n = 3$ at each time point. Two-tailed Mann–Whitney test. $^*P < 0.05$.

anti-ssDNA antibodies, G9gl HL heterozygous mice produced autoantibodies against other nuclear antigens in sera (Fig. 6B–D). For example, 3-month-old G9gl HL heterozygous mice #72 and #78 produced ANAs including anti-RNP and/or anti-SSA antibodies, while #80 had anti-cytoplasmic autoantibodies (Fig. 6C and D). Aged G9gl HL (*Igh*^{b}) × B6. *Igh*^{a}

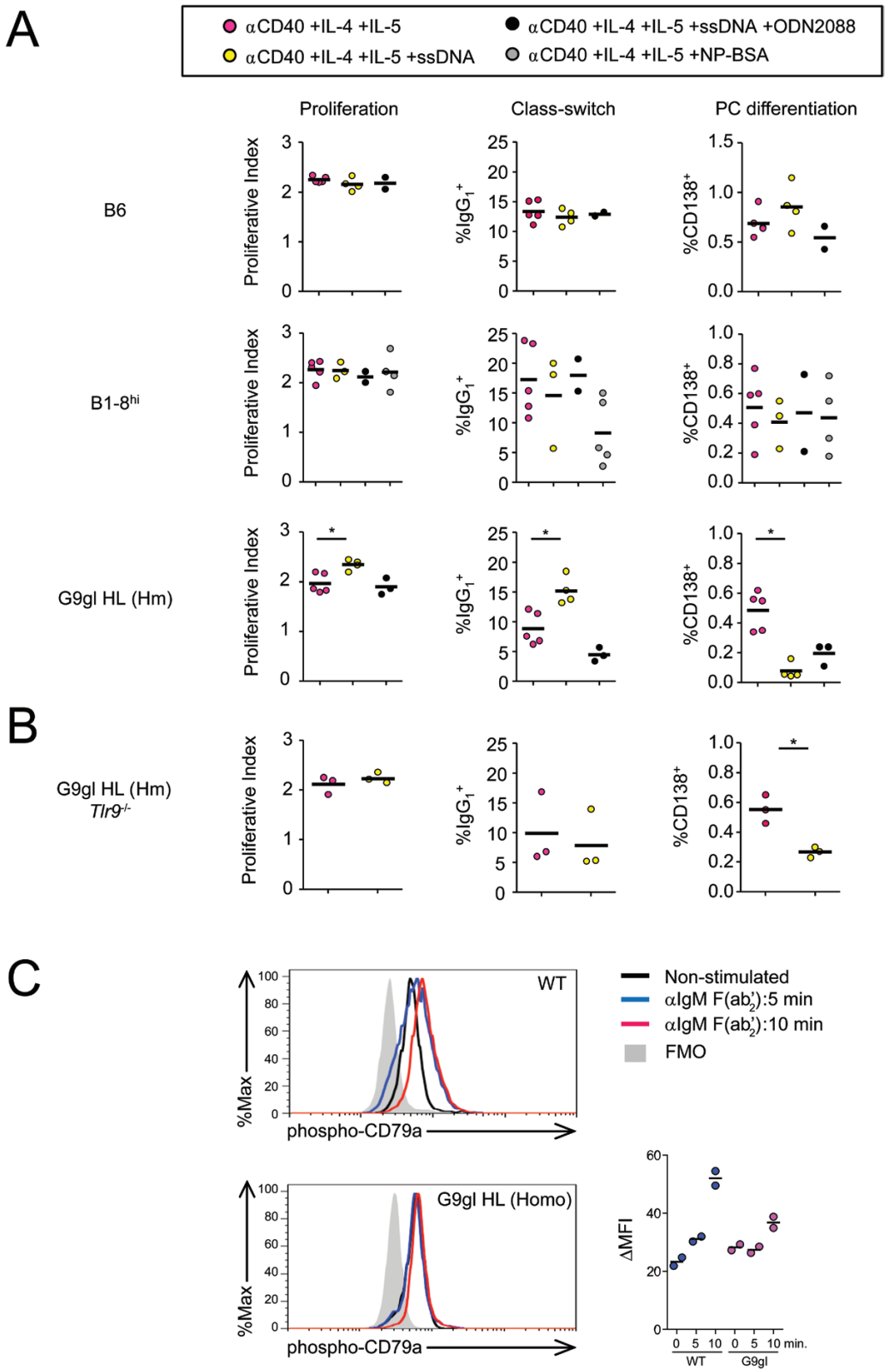

Fig. 5. CpG-containing ssDNA enhances proliferation and CSR, but inhibits plasma cell differentiation. (A and B) Fo B cells from B6, B1-8^{hi}, or G9gl HL homozygous mice (A) or *Tlr9*-deficient G9gl homozygous mice (B) were stimulated *in vitro* with anti-CD40 antibody, IL-4, and IL-5 for 4 d with or without endotoxin-free bacterial ssDNA (1 μg/ml). To antagonize TLR9, 1 μM of ODN2088 (TLR9 antagonist) was added to the culture 1 h before ssDNA stimulation. n = 2–5. Two-tailed Mann–Whitney test. $^*P < 0.05$. (C) Phosphorylated CD79a of Fo B cells from B6 or G9gl HL homozygous mice before or after BCR ligation was detected by intracellular FACS. FACS sorted Fo B cells were stimulated by 10 μg/ml of anti-IgM F(ab')$_2$ for 5 and 10 min. For the histogram, cells were gated for lymphocyte 7AAD$^-$ B220$^+$. ΔMFI is shown in the graph. n = 2 each. The representative results from two experiments are shown.

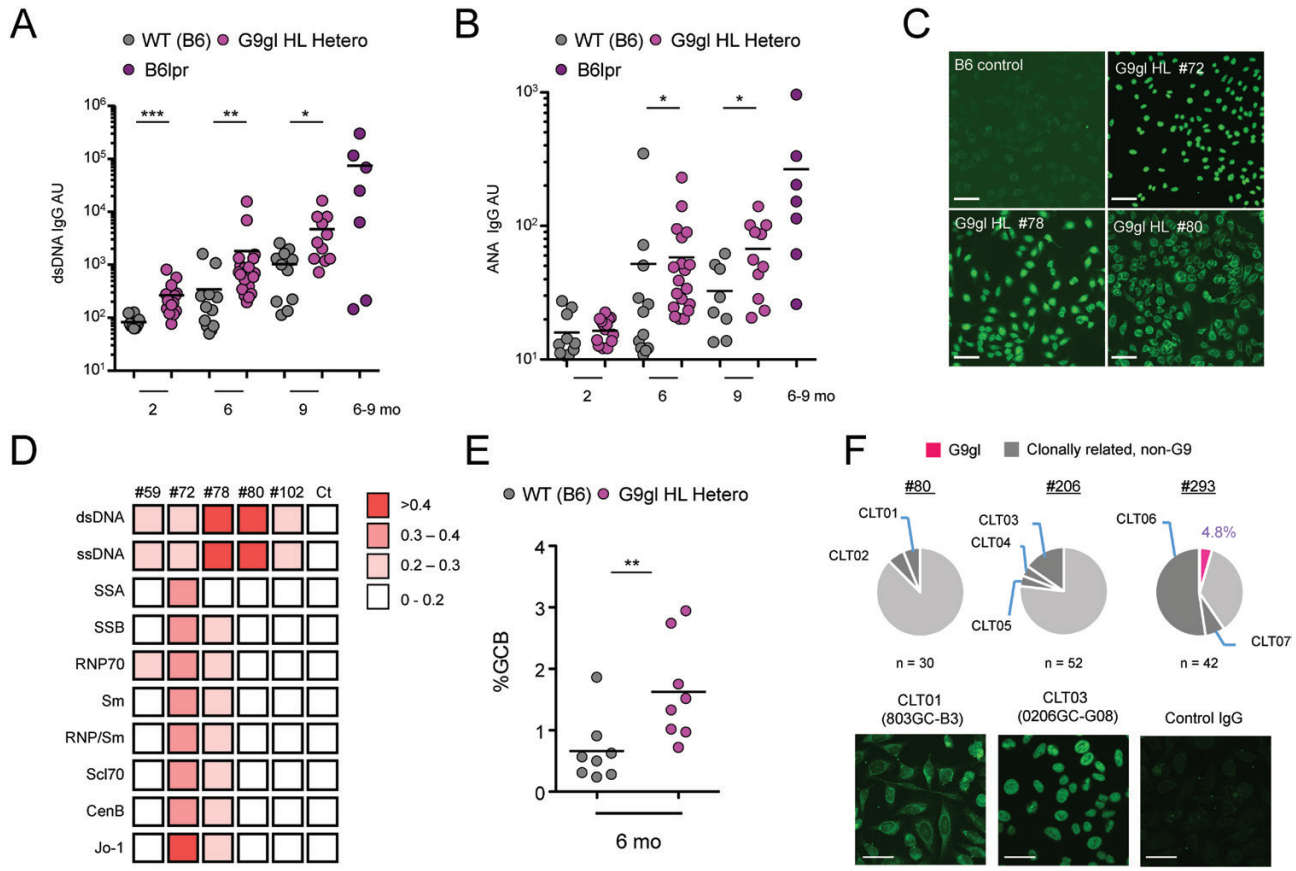

Fig. 6. G9gl B cells fail to enter spontaneous GCs *in vivo*. (A) Serum anti-dsDNA IgG titers in WT, G9gl HL heterozygous (2, 6 and 9 months old), and B6 *Fas*$^{lpr/lpr}$ (B6lpr) mice (6–9 months old) as a positive control. n = 7–19. (B) Serum ANA titers in WT, G9gl HL heterozygous (2, 6 and 9 months old), and B6lpr mice (6–9 months old) as a positive control. n = 7–19. (C) Self-reactivity of sera from representative G9gl HL heterozygous mice with spontaneous anti-dsDNA IgG production at age of 3 months. Sera were diluted in 1:100 and incubated with Hep2 cells on glass slides. Bound IgG was detected by Alexa488-conjugated anti-mouse IgG. (D) Serum IgG reactivity against self-antigens was assessed by self-antigen ELISA. OD450 values are colored as indicated. (E) The proportions of splenic GC B cells in WT and G9gl HL heterozygous mice aged 6 months. n = 7–8 mice. (F) scIg-seq analysis of IgG$^+$ GC B cells from mice with spontaneous autoantibody production at age of 3-10 months. #80, 3 months old, n = 30; #206, 6 months old, n = 52; #293, 10 months old, n = 42. The pie charts indicate the proportion of G9gl B cells (pink) and non-G9gl clonally related B cells (dark gray). Representative sequences in the largest clonotypes from mice #80 and #206 were expressed as recombinant mAbs, and their self-reactivity was tested in Hep2 assays (bottom). (A and C) Two-tailed Mann–Whitney test. $^*P < 0.05$, $^{**}P < 0.01$, $^{***}P < 0.001$. (B and F [bottom]) Bars indicate 50 μm. Representative results from two independent experiments are shown.

heterozygous mice produced WT allele-derived anti-dsDNA IgG_{2a} in sera although the KI allele-derived anti-dsDNA IgG_{2c} titers were elevated in some G9gl HL heterozygous mice, but not statistically significantly (Supplementary Fig. S6). These results suggested that autoantibodies could also be produced by non-G9gl B cells in G9gl heterozygous mice.

This autoantibody production was accompanied by spontaneous germinal center (GC) formation in G9gl HL heterozygous mice (Fig. 6E). To examine the contribution of G9gl B cells to autoantibody production, we performed scIg-seq of IgG$^+$ GC B cells from three G9gl HL heterozygous mice with spontaneous anti-dsDNA IgG production [#80 (3 months), #206 (6 months) and #293 (10 months)]. Unexpectedly, G9gl B cells made up only 4.8% of the GC B fraction in mouse #293 and were undetectable in mice #80 and #206, and the majority of the obtained IgH sequences were non-KI allele-derived IgH (Fig. 6F). Furthermore, the GCs of these mice had clonally related populations, some of which showed self-reactivity when their BCRs were expressed as recombinant antibodies (Fig. 6F). These results indicate that non-G9gl B cells can undergo clonal expansion and differentiate into antibody-secreting cells in the presence of anergic G9gl B cells, which *per se* fail to enter GCs. Similarly, previously reported KI mice expressing anti-ribonuclear complex BCR (594Igi mice) harbored spontaneous GCs that were dominated by non-KI IgH-expressing clonal lineages of B cells and produced autoantibodies to a variety of self-antigens (40).

G9gl B cells fail to enter GCs induced after Treg depletion

Previous studies have suggested that depletion of Tregs induces autoantibody production with activation of anergic B cells (41, 42). To examine whether Treg depletion facilitated activation of G9gl B cells, we generated G9gl HL heterozygous *Foxp3*^{DTR} (G9gl HL *Foxp3*^{DTR}) mice that specifically express a bicistronic cDNA encoding full-length *Foxp3* and human diphtheria toxin receptor (DTR) with eGFP reporter in Tregs (18). Tregs were depleted shortly after DTx administration to

Foxp3^{DTR} and G9gl HL *Foxp3*^{DTR} mice (Fig. 7A–C). G9gl HL *Foxp3*^{DTR} mice produced higher titers of autoantibodies than non-BCR KI *Foxp3*^{DTR} mice, although the total concentration of serum IgG was similar in both groups of mice (Fig. 7D–F). Hep2 staining showed that all G9gl HL *Foxp3*^{DTR} mice produced autoantibodies with anti-cytoplasmic reactivity (Fig. 7G). On days 10 and 24 after DTx administration, there were similar numbers of GC B cells in the spleens of both non-KI *Foxp3*^{DTR} and G9gl HL *Foxp3*^{DTR} mice (Fig. 7H). However, only a small percentage (2.8% and 0% in mice no. F01 and F02, respectively) of GC B cells expressed G9gl BCR, and non-G9gl B cells expanded in splenic GC B cells of G9gl HL *Foxp3*^{DTR} mice at day 24 (Fig. 7I and J). G9gl B cells also made up a minor fraction of memory B cells in these mice (Fig. 7J). There were no G9gl-expressing cells in the PB fraction (Fig. 7J). We also observed a lack of expansion of G9gl B cells in IgG$^+$ GC, IgG$^+$ memory B cells and IgG$^+$ PB from DTx-treated G9gl HL *Foxp3*^{DTR} mice at day 10 (data not shown). Furthermore, G9gl HL homozygous *Foxp3*^{DTR} mice showed no increase in serum anti-dsDNA IgG titers after DTx administration and almost no splenic GC B cells after Treg depletion (Supplementary Fig. S7A and B). These results indicate that G9gl B cells do not differentiate into GC B cells after transient Treg depletion.

Anergic G9gl B cells differentiate into memory B cells in mice immunized with bacteria-derived ssDNA

Since G9gl B cells appeared to be absent from both spontaneously formed GCs and GCs induced by Treg depletion, we next attempted to activate G9gl B cells with cognate antigens and appropriate T-cell help. An earlier study showed that mBSA-conjugated bacterial DNA immunization induced anti-dsDNA antibody production in non-autoimmune mice

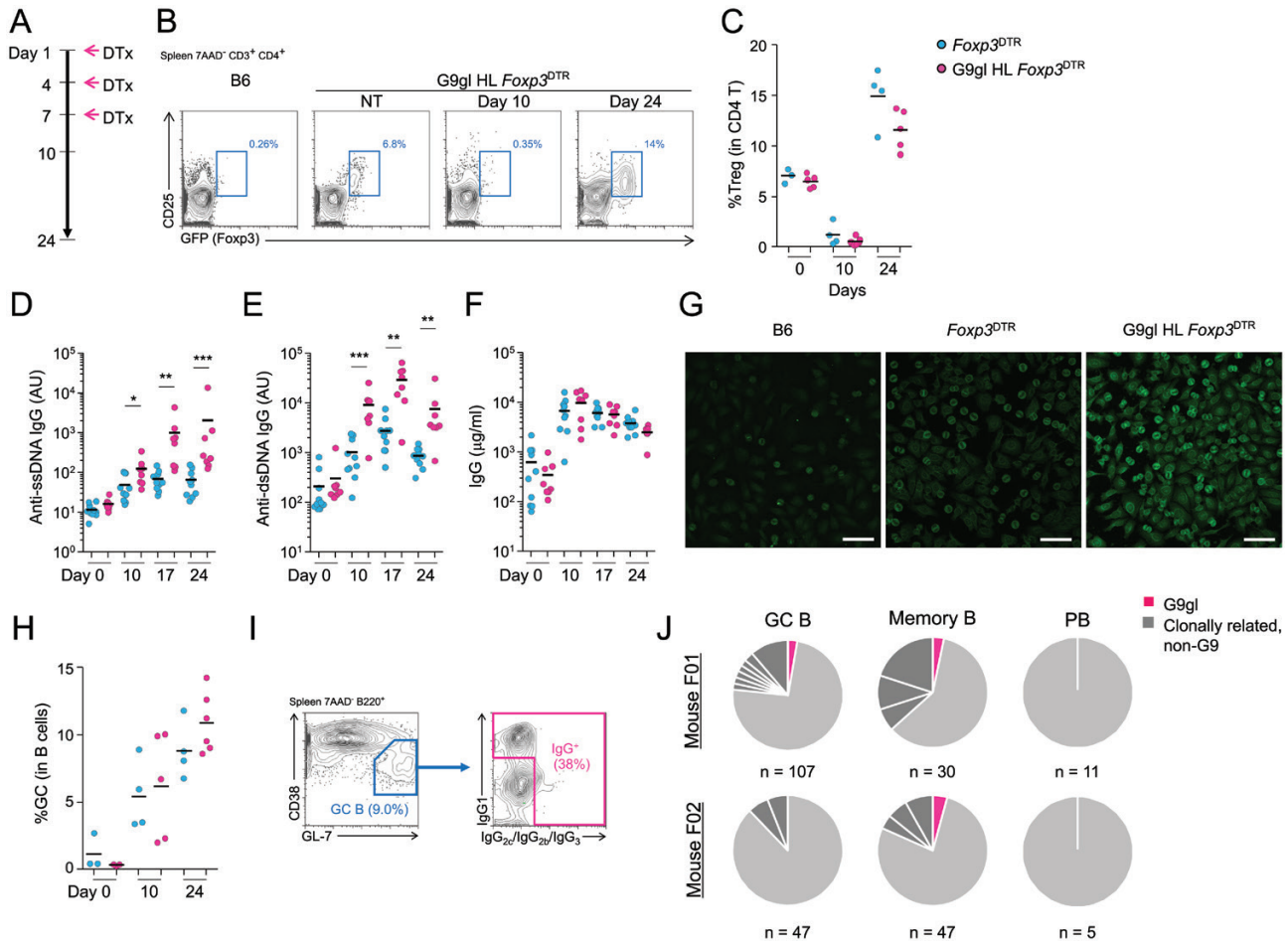

Fig. 7. G9gl B cells fail to enter GCs after transient Treg depletion. (A) Experimental protocol to deplete Tregs. *Foxp3*^{DTR} or *Foxp3*^{DTR} G9gl HL heterozygous mice were intraperitoneally administered 1 μg of diphtheria toxin (DTx) on days 1, 4, and 7. (B) Representative FACS plot of Tregs (CD4$^+$ CD25$^+$ GFP$^+$). Gating for 7AAD$^-$ CD3$^+$ CD4$^+$. Splenocytes from WT B6 are shown as a negative control. (C) The percentages of Tregs in the spleens of *Foxp3*^{DTR} or *Foxp3*^{DTR} G9gl HL heterozygous mice on days 0, 10, and 24 after DTx administration. (D) Anti-ssDNA IgG titers. (E) Anti-dsDNA IgG titers. (F) Total IgG concentrations in sera of each group on days 0, 10, 17, and 24 after DTx administration. (G) Representative results of a Hep2 staining assay with sera (100-diluted) from WT, *Foxp3*^{DTR}, or *Foxp3*^{DTR} G9gl HL heterozygous mice on day 24. Bar indicates 100 μm. Representative results from two independent experiments are shown. (H) The proportions of GC B cells in the spleens of *Foxp3*^{DTR} or *Foxp3*^{DTR} G9gl HL heterozygous mice on days 0, 10, and 24 after DTx administration. (I) Gating strategy of IgG$^+$ GC B cells for scIg-seq. (J) Frequencies of G9gl B cells in IgG$^+$ GC B, IgG$^+$ memory B cells, and IgG$^+$ PBs. IgG$^+$ GC B cells (F01, n = 107; F02, n = 47), IgG$^+$ memory B cells (B220$^+$ CD38^{hi} GL7^{lo} IgG$^+$) (F01, n = 30; F02, n = 47), and PBs (B220$^{+/lo}$ CD138$^+$ IgG$^+$, F01, n = 11; F02, n = 5) were sorted for scIg-seq on day 24 after DTx administration. (C–F and H) Two-tailed Mann–Whitney test. *P < 0.05; **P < 0.01; ***P < 0.001.

(33). We immunized G9gl HL heterozygous mice with *E. coli*-derived plasmid DNA (bacDNA) that was heat-denatured and conjugated with mBSA. As shown in Fig. 8A and B, anti-dsDNA IgG titers were robustly elevated in both WT and G9gl HL heterozygous mice after mBSA-conjugated bacDNA immunization, but not after immunization with bacDNA alone. The prime-boost with mBSA-conjugated bacDNA induced IgG$^+$ GC B cells, IgG$^+$ memory B cells and IgG$^+$ PBs in G9gl HL heterozygous mice (Fig. 8C and D and Supplementary Fig. S8). To evaluate the frequency of G9gl B cells in each B-cell subset, we performed scIg-seq. Although G9gl BCR-expressing clones were hardly detectable in the IgG$^+$ GC B cell and IgG$^+$ PB fractions, about 5% and 18% of G9gl BCR-expressing clones were isolated from the IgG$^+$ memory B-cell fraction on days 7 and 35, respectively (Fig. 8E). Notably, one-third of the obtained G9gl H chain sequences were somatically mutated (Fig. 8F and Supplementary Fig. S9), although these BCRs did not show any dsDNA reactivity when expressed as monoclonal antibodies (data not shown). This indicates that they may have transiently undergone a GC reaction or acquired mutations via the extrafollicular pathway. However, mBSA-conjugated bacDNA immunization activated G9gl B cells to undergo CSR and memory B-cell differentiation, but not PB differentiation. Thus, G9gl B cells can differentiate into memory B cells when stimulated by cognate antigens with concomitant induction by helper T cells.

Discussion

It has not been fully clarified whether B cells expressing germline precursors of self-reactive antibodies, particularly patient-derived high-affinity anti-dsDNA antibodies, are negatively regulated by tolerance checkpoints and what conditions are required for activation of such B cells although a few studies using KI mice expressing only the reversely mutated germline H chain of an NZB/W-derived anti-dsDNA antibody were reported (14, 43). In this study, we sought to determine whether the germline precursor B cells of SLE patient-derived pathogenic anti-dsDNA B cells are subjected to tolerance mechanisms. To this end, we generated a novel site-directed KI mouse line, G9gl that harbors reversely mutated H and L chains from a lupus patient-derived high-affinity anti-dsDNA mAb, 121G9 (5). Here we showed that G9gl B cells were readily subjected to immune tolerance like fully self-reactive B cells. They were eliminated by receptor editing, rendered anergic and rigorously excluded from GC reactions. Furthermore, upon stimulation of a self-antigen and appropriate T-cell help, they could differentiate into memory B cells, but still failed to differentiate into plasma cells. These findings indicate that not only generation, but also activation of low-affinity anti-ssDNA precursor B cells were suppressed by multiple layers of immune tolerance checkpoints.

Despite the presence of the pre-rearranged V_H–D_H–J_H fragment, half of the B cells in G9gl HL heterozygous mice expressed H chains encoded by the WT allele. This was due to receptor editing by V_H replacement, in which RAG-mediated DNA rearrangement occurs at a 7-bp cryptic recombination signal sequence (3′-TACTGTG-5′) at the 3′ end of G9gl V_H. Although V_H replacement may eliminate self-reactive H chains, as previously suggested (35), it can provide a mechanism to modify unwanted V_H–D_H–J_H regions (44, 45). Because of the lower efficiency compared with canonical V_H to D_H–J_H recombination (45, 46), V_H replacement may contribute to the reduction of peripheral B cells in G9gl HL KI mice.

In the periphery, G9gl B cells were rendered anergic. G9gl B cells had reduced BCR expression on the surface and a shortened half-life, both features that were commonly observed in previously reported self-reactive B cells (47). In global gene expression analysis, the upregulated genes in G9gl B cells were also present in B cells from previously reported self-reactive models (38). In particular, upregulation of genes related to B-cell activation, cell cycling and apoptosis indicated that G9gl B cells may undergo activation-induced cell death. In this way, they resemble anti-dsDNA 3H9/λ$^+$ B cells in non-autoimmune mice, which showed active proliferation with an increased turnover rate in the periphery (13). On the other hand, although receptor desensitization is a hallmark of anergic B cells (48), G9gl B cells in this study could provide signals after BCR cross-linking. Differences in anergic phenotypes between individual mouse models may be attributed to the availability of self-antigens and the antigen affinity of self-reactive BCRs (48, 49). We assume that the anti-ssDNA reactivity of G9gl B cells in the present study is much lower than that in previously reported self-reactive BCR models. Thus, the low-affinity ssDNA reactivity of G9gl BCR not only confers typical anergy, but also the unique phenotype of G9gl B cells.

Concomitantly with spontaneous GC formation in the spleen, G9gl HL heterozygous mice produced various autoantibodies reactive not only to DNA, but also to other self-antigens. This phenomenon, known as epitope spreading, has also been observed in self-reactive 564Igi BCR KI mice (40). Spontaneous autoantibody production was further accelerated by transient depletion of Tregs. Nonetheless, the vast majority of GC B cells harbored BCRs derived from the non-KI allele in G9gl HL heterozygous mice that produced serum autoantibodies, suggesting that G9gl B cells could not participate in the GC reaction. Functional anergy may restrain G9gl B cells from entering the GC reaction. If this is the case, self-reactive GC B cells carrying non-G9gl KI BCR could originate from non-anergic precursors that presumably have much lower self-reactivity than G9gl B cells. Although the precise mechanisms that induce self-reactive GCs in the heterozygous G9gl HL KI mice remain to be determined, anergic G9gl B cells might efficiently present self-antigens to helper T cells to initiate self-reactive GCs.

We found that immunization of G9gl HL KI mice with mBSA-conjugated bacDNA induced GCs in which the frequency of G9gl B cells was negligible. However, G9gl B cells accounted for a sizable fraction (~18%) of IgG$^+$ memory B cells in mice immunized with mBSA-conjugated bacDNA, indicating that cognate antigen stimulation with T helper cell involvement leads to differentiation of G9gl B cells into switched memory B cells without robust expansion in GCs. Since about one-third of the G9gl memory B cells harbored somatically mutated Igs, they might have transiently entered GCs. Alternatively, G9gl B cells may acquire somatic mutations via the extrafollicular pathway. Despite multiple administrations of ssDNA in the immunization regimen, there were hardly any G9gl B cells in the splenic PB fraction,

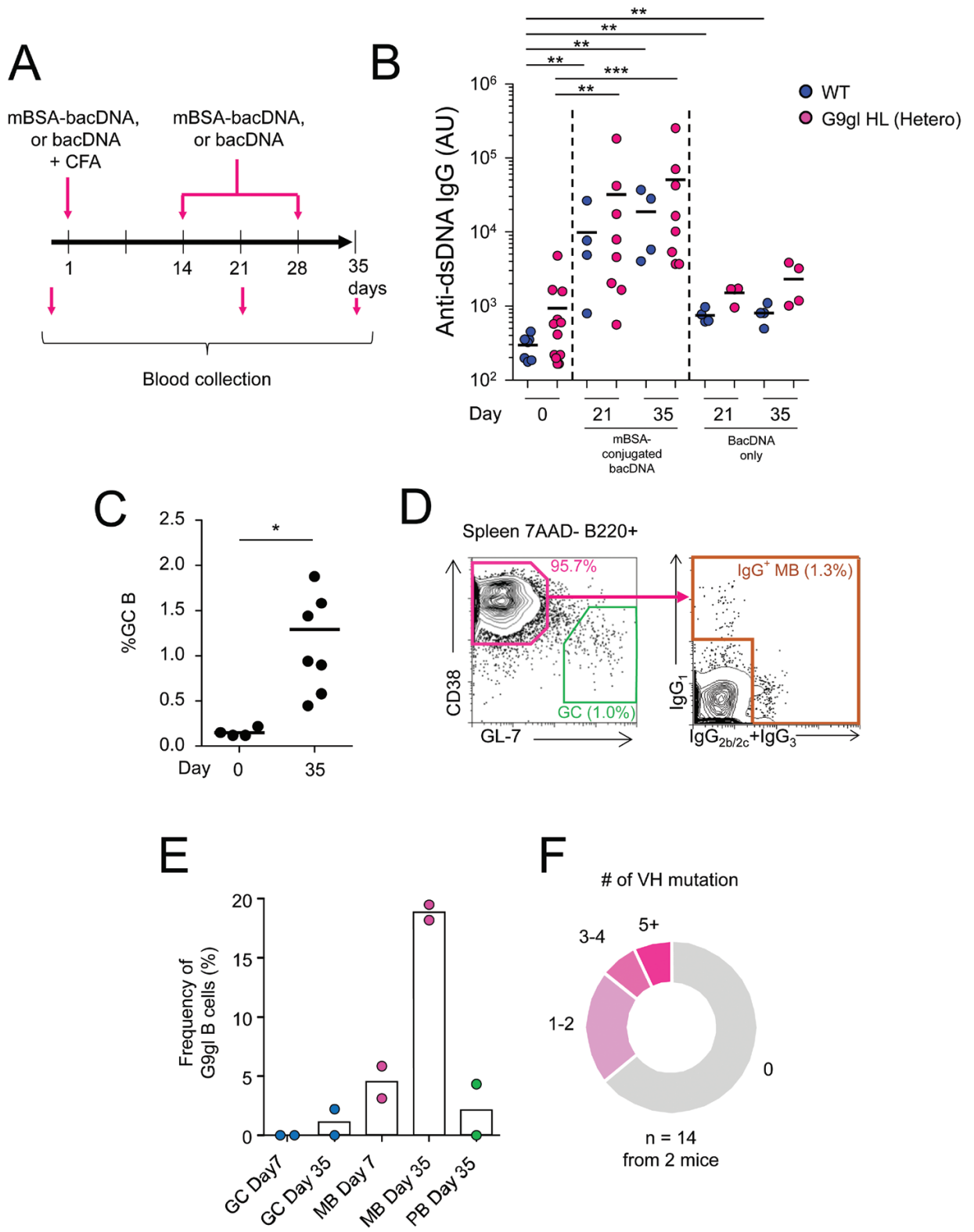

Fig. 8. G9gl B cells differentiate into memory B cells in mice immunized with bacteria-derived ssDNA. (A) Experimental regimen for mBSA-bacDNA immunization. (B) Serum anti-dsDNA IgG titers. (C) Frequencies of GC B in spleens of unimmunized and immunized G9gl HL heterozygous mice (day 35). (D) Gating strategy of IgG$^+$ memory B (MB) cells for scIg-seq. (E) Frequencies of G9gl B cells in the splenic IgG$^+$ GC B, IgG$^+$ memory B (MB) cell, and IgG$^+$ PB fractions of G9gl HL heterozygous mice immunized with mBSA-conjugated bacDNA (days 7 and 35) determined by scIg-seq. Data from two mice in individual categories are shown (GC B day 7, n = 46 and 33; GC B day 35, n = 45 and 39; MB day 7, n = 32 and 17; MB day 35, n = 41 and 33; PB day 35, n = 10 and 23). (F) The number of somatic mutations in the G9gl H chain obtained from IgG$^+$ memory B cells in immunized G9gl HL heterozygous mice (day 35, n = 14 from 2 mice).

indicating that G9gl memory B cells failed to differentiate into PBs. This may reflect the culture assay results showing that bacterial ssDNA enhanced proliferation and CSR, but suppressed plasma cell differentiation of G9gl B cells independently of TLR9. It was recently reported that persistent *bcl-2* overexpression in post-GC B cells resulted in accumulation of nucleosome-reactive memory B cells and splenic PBs in aged non-autoimmune mice, indicating the presence of an apoptosis-dependent tolerance checkpoint in post-GC B cells (50). However, our results suggest that ssDNA ligation to BCR rather inhibits plasma cell differentiation of memory B cells expressing low-affinity anti-ssDNA BCRs through altered signaling characterized by impaired phosphorylation of CD79a and inefficient calcium mobilization.

We demonstrated that low-affinity B cells that were precursors of pathogenic anti-dsDNA antibody-producing cells were readily subjected to immune tolerance. Thus, dysfunctional tolerance checkpoints may be a prerequisite for the development of SLE as previously indicated (51, 52). Alternatively, low-affinity ssDNA-reactive precursors like G9gl B cells may pass through immune tolerance checkpoints in humans, which could allow the precursor B cells to undergo somatic hypermutation and antigen-driven selection.

In sum, our study demonstrated that low-affinity germline precursor B cells were restrained at multiple tolerance checkpoints, in particular at the entry of GCs. A future study will be required to identify the factors responsible for restricting GC maturation of low-affinity precursor B cells.

Funding

This work was supported by Grant-in-Aid for Scientific Research from Japan Society for the Promotion of Science (JSPS), grant no 16K08837 and 19K07622 (to S.S.) and Takeda Science Foundation (to S.S.) and Kishimoto Foundation (to H.K).

Acknowledgements

We thank Nana Iwami, Kazuya Takeda and Jun Katayama (IFReC, Osaka University) for their assistance with experiments; Drs Saki Nishioka (NPO for Biotechnology Research and Development, Suita, Osaka) and Kazuhiko Kaseda (RIMD, Osaka University) for their assistance in generating the G9gl mouse line; Keiko Murata (RIMD, Osaka University), Yuki Uchikawa, and Yuko Kabumoto (IFReC, Osaka University) for DNA sequencing and cell sorting; RBC, Riken for B6.*Igh*^{a} mice; Alexander Rudensky for *Foxp*3-DTR mice; and Shizuo Akira (IFReC, Osaka University) for *Tlr9* KO.

Conflicts of interest statement: the authors declared no conflicts of interest.

References

1 Isenberg, D. A., Manson, J. J., Ehrenstein, M. R. and Rahman, A. 2007. Fifty years of anti-ds DNA antibodies: are we approaching journey's end? *Rheumatology (Oxford)* 46:1052.
2 Rekvig, O. P. 2019. The dsDNA, anti-dsDNA antibody, and lupus nephritis: what we agree on, what must be done, and what the best strategy forward could be. *Front. Immunol.* 10:1104.
3 Kalsi, J., Ravirajan, C. T., Rahman, A. and Isenberg, D. A. 1999. Structure-function analysis and the molecular origins of anti-DNA antibodies in systemic lupus erythematosus. *Expert Rev. Mol. Med.* 1999:1.
4 Pavlovic, M., Kats, A., Cavallo, M. *et al.* 2010. Pathogenic and epiphenomenal anti-DNA antibodies in SLE. *Autoimmune Dis.* 2011:462841.
5 Sakakibara, S., Arimori, T., Yamashita, K. *et al.* 2017. Clonal evolution and antigen recognition of anti-nuclear antibodies in acute systemic lupus erythematosus. *Sci. Rep.* 7:16428.
6 Herron, J. N., He, X. M., Ballard, D. W. *et al.* 1991. An autoantibody to single-stranded DNA: comparison of the three-dimensional structures of the unliganded Fab and a deoxynucleotide-Fab complex. *Proteins* 11:159.
7 Tanner, J. J., Komissarov, A. A. and Deutscher, S. L. 2001. Crystal structure of an antigen-binding fragment bound to single-stranded DNA. *J. Mol. Biol.* 314:807.
8 Shlomchik, M., Mascelli, M., Shan, H. *et al.* 1990. Anti-DNA antibodies from autoimmune mice arise by clonal expansion and somatic mutation. *J. Exp. Med.* 171:265.
9 Guo, W., Smith, D., Aviszus, K. *et al.* 2010. Somatic hypermutation as a generator of antinuclear antibodies in a murine model of systemic autoimmunity. *J. Exp. Med.* 207:2225.
10 Wellmann, U., Letz, M., Herrmann, M. *et al.* 2005. The evolution of human anti-double-stranded DNA autoantibodies. *Proc. Natl Acad. Sci. USA* 102:9258.
11 Erikson, J., Radic, M. Z., Camper, S. A. *et al.* 1991. Expression of anti-DNA immunoglobulin transgenes in non-autoimmune mice. *Nature* 349:331.
12 Radic, M. Z., Mascelli, M. A., Erikson, J. *et al.* 1991. Ig H and L chain contributions to autoimmune specificities. *J. Immunol.* 146:176.
13 Mandik-Nayak, L., Bui, A., Noorchashm, H. *et al.* 1997. Regulation of anti-double-stranded DNA B cells in nonautoimmune mice: localization to the T-B interface of the splenic follicle. *J. Exp. Med.* 186:1257.
14 Pewzner-Jung, Y., Friedmann, D., Sonoda, E. *et al.* 1998. B cell deletion, anergy, and receptor editing in "knock in" mice targeted with a germline-encoded or somatically mutated anti-DNA heavy chain. *J. Immunol.* 161:4634.
15 Fields, M. L., Hondowicz, B. D., Wharton, G. N. *et al.* 2005. The regulation and activation of lupus-associated B cells. *Immunol. Rev.* 204:165.
16 Fields, M. L. and Erikson, J. 2003. The regulation of lupus-associated autoantibodies: immunoglobulin transgenic models. *Curr. Opin. Immunol.* 15:709.
17 Hemmi, H., Takeuchi, O., Kawai, T. *et al.* 2000. A Toll-like receptor recognizes bacterial DNA. *Nature* 408:740.
18 Kim, J. M., Rasmussen, J. P. and Rudensky, A. Y. 2007. Regulatory T cells prevent catastrophic autoimmunity throughout the lifespan of mice. *Nat. Immunol.* 8:191.
19 Shih, T. A., Meffre, E., Roederer, M. and Nussenzweig, M. C. 2002. Role of BCR affinity in T cell dependent antibody responses in vivo. *Nat. Immunol.* 3:570.
20 Ran, F. A., Hsu, P. D., Wright, J. *et al.* 2013. Genome engineering using the CRISPR-Cas9 system. *Nat. Protoc.* 8:2281.
21 Mashiko, D., Fujihara, Y., Satouh, Y. *et al.* 2013. Generation of mutant mice by pronuclear injection of circular plasmid expressing Cas9 and single guided RNA. *Sci. Rep.* 3:3355.
22 Fujihara, Y., Kaseda, K., Inoue, N. *et al.* 2013. Production of mouse pups from germline transmission-failed knockout chimeras. *Transgenic Res* 22:195.
23 Lee, S.-H. 2013. Flow cytometric analysis of calcium influx assay in T cells. *Bio-protocol* 3:e910.
24 Sakakibara, S., Yasui, T., Jinzai, H. *et al.* 2020. Self-reactive and polyreactive B cells are generated and selected in the germinal center during γ-herpesvirus infection. *Int. Immunol.* 32:27.
25 von Boehmer, L., Liu, C., Ackerman, S. *et al.* 2016. Sequencing and cloning of antigen-specific antibodies from mouse memory B cells. *Nat. Protoc.* 11:1908.
26 Rohatgi, S., Ganju, P. and Sehgal, D. 2008. Systematic design and testing of nested (RT-)PCR primers for specific amplification of mouse rearranged/expressed immunoglobulin variable region genes from small number of B cells. *J. Immunol. Methods* 339:205.
27 Lefranc, M. P., Giudicelli, V., Duroux, P. *et al.* 2015. IMGT®, the international ImMunoGeneTics information system® 25 years on. *Nucleic Acids Res.* 43(Database issue):D413.
28 Isenberg, D. A., Dudeney, C., Williams, W. *et al.* 1987. Measurement of anti-DNA antibodies: a reappraisal using five different methods. *Ann. Rheum. Dis.* 46:448.

29 Parajuli, G., Tekguc, M., Wing, J. B. *et al.* 2021. Arid5a promotes immune evasion by augmenting tryptophan metabolism and chemokine expression. *Cancer Immunol. Res.* 9:862.
30 Mootha, V. K., Lindgren, C. M., Eriksson, K. F. *et al.* 2003. PGC-1alpha-responsive genes involved in oxidative phosphorylation are coordinately downregulated in human diabetes. *Nat. Genet.* 34:267.
31 Subramanian, A., Tamayo, P., Mootha, V. K. *et al.* 2005. Gene set enrichment analysis: a knowledge-based approach for interpreting genome-wide expression profiles. *Proc. Natl Acad. Sci. USA* 102:15545.
32 Krämer, A., Green, J., Pollard, J. Jr and Tugendreich, S. 2014. Causal analysis approaches in ingenuity pathway analysis. *Bioinformatics* 30:523.
33 Gilkeson, G. S., Grudier, J. P., Karounos, D. G. and Pisetsky, D. S. 1989. Induction of anti-double stranded DNA antibodies in normal mice by immunization with bacterial DNA. *J. Immunol.* 142:1482.
34 Merrell, K. T., Benschop, R. J., Gauld, S. B. *et al.* 2006. Identification of anergic B cells within a wild-type repertoire. *Immunity* 25:953.
35 Chen, C., Nagy, Z., Prak, E. L. and Weigert, M. 1995. Immunoglobulin heavy chain gene replacement: a mechanism of receptor editing. *Immunity* 3:747.
36 Sekiguchi, D. R., Eisenberg, R. A. and Weigert, M. 2003. Secondary heavy chain rearrangement: a mechanism for generating anti-double-stranded DNA B cells. *J. Exp. Med.* 197:27.
37 Goodnow, C. C., Brink, R. and Adams, E. 1991. Breakdown of self-tolerance in anergic B lymphocytes. *Nature* 352:532.
38 Glynne, R., Ghandour, G., Rayner, J. *et al.* 2000. B-lymphocyte quiescence, tolerance and activation as viewed by global gene expression profiling on microarrays. *Immunol. Rev.* 176:216.
39 Getahun, A., Beavers, N. A., Larson, S. R. *et al.* 2016. Continuous inhibitory signaling by both SHP-1 and SHIP-1 pathways is required to maintain unresponsiveness of anergic B cells. *J. Exp. Med.* 213:751.
40 Degn, S. E., van der Poel, C. E., Firl, D. J. *et al.* 2017. Clonal evolution of autoreactive germinal centers. *Cell* 170:913.
41 Leonardo, S. M., Josephson, J. A., Hartog, N. L. and Gauld, S. B. 2010. Altered B cell development and anergy in the absence of Foxp3. *J. Immunol.* 185:2147.
42 Liu, Y., Liu, A., Iikuni, N. *et al.* 2014. Regulatory CD4+ T cells promote B cell anergy in murine lupus. *J. Immunol.* 192:4069.
43 Huang, W., Moisini, I., Bethunaickan, R. *et al.* 2011. BAFF/APRIL inhibition decreases selection of naive but not antigen-induced autoreactive B cells in murine systemic lupus erythematosus. *J. Immunol.* 187:6571.
44 Zhang, Z., Burrows, P. D. and Cooper, M. D. 2004. The molecular basis and biological significance of VH replacement. *Immunol. Rev.* 197:231.
45 Koralov, S. B., Novobrantseva, T. I., Königsmann, J. *et al.* 2006. Antibody repertoires generated by VH replacement and direct VH to JH joining. *Immunity* 25:43.
46 Zhang, Z. 2007. VH replacement in mice and humans. *Trends Immunol.* 28:132.
47 Brink, R. and Phan, T. G. 2018. Self-reactive B cells in the germinal center reaction. *Annu. Rev. Immunol.* 36:339.
48 Cambier, J. C., Gauld, S. B., Merrell, K. T. and Vilen, B. J. 2007. B-cell anergy: from transgenic models to naturally occurring anergic B cells? *Nat. Rev. Immunol.* 7:633.
49 Ferry, H., Jones, M., Vaux, D. J. *et al.* 2003. The cellular location of self-antigen determines the positive and negative selection of autoreactive B cells. *J. Exp. Med.* 198:1415.
50 Mayer, C. T., Nieke, J. P., Gazumyan, A. *et al.* 2020. An apoptosis-dependent checkpoint for autoimmunity in memory B and plasma cells. *Proc. Natl Acad. Sci. USA* 117:24957.
51 Yurasov, S., Wardemann, H., Hammersen, J. *et al.* 2005. Defective B cell tolerance checkpoints in systemic lupus erythematosus. *J. Exp. Med.* 201:703.
52 Meffre, E. and O'Connor, K. C. 2019. Impaired B-cell tolerance checkpoints promote the development of autoimmune diseases and pathogenic autoantibodies. *Immunol. Rev.* 292:90.